Attosecond light-pulse-induced photoassociation

Paula Rivière, Camilo Ruiz, and Jan-Michael Rost
Max-Planck Institute for the Physics of Complex Systems, Nöthnitzer Strasse 38, D-01187 Dresden, Germany
(Received 31 January 2008; published 26 March 2008; publisher error corrected 9 April 2008)

We explore stimulated photoassociation in the context of attosecond pump-probe schemes of atomic matter. An attosecond pulse—the probe—is used to induce photoassociation of an electronic wave packet which had been created before, typically with an attosecond pump pulse at an atomic center different from the one of photoassociation. We will show that the electron absorption is maximal for a certain delay between the pulses. Two ways of enhancing and controlling stimulated photoassociation are proposed, namely, using an additional infrared pulse to steer the electronic wave packet and using a train of attosecond pulses instead of a single pair. A direct application of ultrafast stimulated photoassociation is the measurement of atomic distances.

DOI: 10.1103/PhysRevA.77.033421 PACS number(s): 32.80.Rm, 42.50.Hz

I. INTRODUCTION

Attosecond laser pulses hold the promise to be a tool to image structure of matter on the atomic scale with unprecedented temporal and spatial resolution [1–3]. Nowadays, attosecond pulses with a typical duration of electronic motion in atoms or molecules [4] can be produced and characterized in a controlled way [5], and are therefore ready to be used for mapping and controlling electronic motion [6,7]. First applications of attosecond pulses have focused on the generation of attosecond electron wave packets, e.g., for real time observation of tunneling [8], the interference of wave packets using attosecond trains [9], or to obtain autoionization widths [10]. They have also been used for imaging molecular orbitals [11]. All the applications show that the role of attosecond pulses has been restricted so far to study ionization or interference processes. Here we propose a new application of attosecond pulses: the recapture of a continuum electron by an ion, induced by an attosecond pulse. This constitutes a new process of photoassociation, namely, induced photoassociation (IPA). Although it is a process of stimulated photoabsorption triggered by the attosecond photon field, it has low probability due to the small time span of the attosecond pulse during which the IPA is possible.

Hence, after the demonstration of the basic process of IPA we will also discuss how the reabsorption probability can be enhanced. This can be achieved by using an attosecond pulse train, which delivers a series of pairs of pump-probe pulses. The drawback of such a technique is that the time delay between two attosecond pulses is typically not variable in an experiment. However, adding an infrared (IR) pulse can achieve in the context of IPA the same effect as changing the delay between the attosecond pulses, namely, controlling the time when the electronic wave packet arrives at the atomic center by which it is supposed to be captured. This will be shown explicitly for one attosecond pulse per IR cycle, which is experimentally achievable [12].

Since this work is mainly intended to introduce the concept of IPA, we restrict ourselves to the simplest possible scenario, two ions and an electron, and to be specific, we take H_2^+. Furthermore, we carry out fully time-dependent quantum calculations in one and two spatial dimensions.

The paper is organized as follows. In Sec. II we introduce our Hamiltonian and describe how we solve the electron dynamics. In Sec. III we describe the basic IPA process with two attosecond pulses. In Sec. IV we discuss how the addition of an IR pulse changes the dynamics. Section V presents the results for an attosecond pulse train in combination with an IR pulse, and Sec. VI contains the conclusions and outlook of the paper. Atomic units are used unless stated otherwise.

II. TIME-DEPENDENT ONE-ELECTRON QUANTUM DYNAMICS IN A LANDSCAPE OF ATTRACTIVE POTENTIALS

As mentioned before, for the sake of clarity of the concept, we consider the simplest possible dynamical situation for IPA to occur in a pump-probe setting with the ions (protons) fixed in space. We have in mind the idealized situation that an electron, bound to one proton (forming hydrogen) is ionized by the first attopulse. The electron packet propagates and part of it is recaptured subsequently at another proton, assisted by a second attopulse. The recapture is maximal if the probe pulse comes at the time when the center of the wave packet is at the second proton.

The fixed nuclei assumption is a twofold but well justified approximation. First, the situation of a hydrogen atom and a proton separated by 40 a.u. as considered below, is naturally created by exciting the H_2^+ molecule from its ground state, with equilibrium internuclear distance $R_0=2$, to a dissociative state. This leads to a maximum nuclear kinetic energy determined by the energy of this state, which is $V_{2p\sigma_u}(R_0)=-0.169$. At a distance $R=40$, the potential energy approaches $V_{2p\sigma_u}(\infty)=-0.5$. The difference determines the maximum kinetic energy, $Mv^2/4=V_{2p\sigma_u}(R_0)-V_{2p\sigma_u}(\infty)$. Hence the relative velocity of the two nuclei with mass $M=1836$ is $v\sim 0.0268$, so that the nuclei move around one atomic unit during a typical pump-probe interval of about 50 a.u. Even smaller is the motion due to the IPA process itself, i.e., due to the Coulomb repulsion of the two protons after the first (ionizing) attosecond pulse.

We assume the light field to be linearly polarized along the x axis (unit vector $\hat{x}$),

$$\boldsymbol{E}(t) = \hat{x}E_0\left[\sin(\omega t)\sin^2\left(\frac{\omega t}{2N}\right) + \sin(\omega t')\sin^2\left(\frac{\omega t'}{2N}\right)\right], \quad (1)$$

where $t' = t - \Delta t$ and Δt is the delay between the two attosecond pulses, which have a central frequency ω and a duration of N cycles. The Hamiltonian reads

$$H = \frac{\boldsymbol{p}^2}{2} + V + p_x A(t)/c \equiv H_0 + p_x A(t)/c, \quad (2)$$

where $A(t) = -c\int^t E(t')dt'$. Furthermore, we consider only the case where the two protons are fixed on the x axis at distances $\pm x_0$ with $x_0 = 20$, so that the soft-core potential reads in two dimensions $V(x,y) = W_-(x,y) + W_+(x,y)$ with

$$W_\pm(x,y) = -[(x \mp x_0)^2 + y^2 + \epsilon]^{-1/2}. \quad (3)$$

The softening parameter ϵ, adjusted to provide a ground state energy of $E_g = -0.5$ for the isolated H atom, is $\epsilon_{1D} = 2.0$ and $\epsilon_{2D} = 0.63$ in one and two dimensions, respectively. The ground state energy corresponds to an isolated hydrogen atom, which is approximately true for the second proton at a distance of 40 a.u. To localize the state at one nucleus, one has to take superpositions of the ground states of gerade and ungerade symmetry, $\psi_{g/u}$, which are formally the ground and first excited state of the system. This is well known from ion-atom collisions,

$$\psi_\pm = (\psi_g \pm \psi_u)/\sqrt{2}, \quad (4)$$

where we define ψ_+ to be localized at the right well $W_+(x,y)$ at $x_0 = +20$ of Eq. (3) [19].

The initial state is propagated numerically in time under the Hamiltonian of Eq. (2) using the Crank-Nicholson method with a time step of $\delta t = 0.05$. The grid ranges from -100 to $+100$, with a spatial step $\delta x = 0.1$. The eigenstates $\psi_{g/u}$ from Eq. (4) are computed using imaginary time propagation under the Hamiltonian H_0 from Eq. (2).

III. TWO ATTOSECOND PULSES

In this section we will investigate under which conditions induced photoassociation can be realized within the framework of a dual attosecond pulse pump-probe scenario [13]. For simplicity, we will assume that at the beginning the electron is always well localized around x_0 in the well W_+ with initial wave function $\psi_+(t=0)$. Asymmetric dissociative states can be realized (with an electron localization probability up to 84%) by means of laser-assisted dissociation [7]. We use three different wavelengths (40, 60, and 80 nm), and high intensity attosecond pulses ($I = 10^{16}$ W/cm^2) in order to obtain good statistics for IPA.

For optimum recombination, the main velocity v of the electron wave packet, the delay Δt between the pulses and the distance $2x_0$ between the two atomic centers must fulfill roughly the classical relation $v = 2x_0/\Delta t$. More precisely, since the electron absorbs one photon of energy ω from the pump pulse, energy conservation can be used to determine the electron velocity of the center of the wave packet classically for a calculated electron trajectory $\boldsymbol{r}(t)$. With the Hamiltonian H from Eq. (2) we have, for $t > 2\pi N/\omega$,

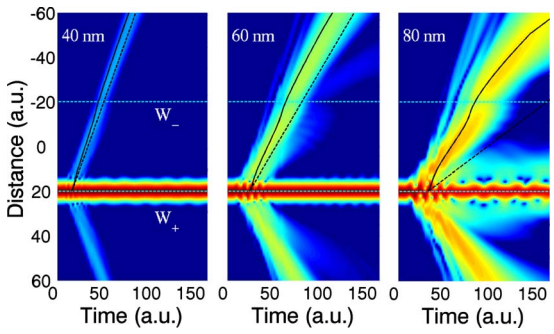

FIG. 1. (Color online) Electron density as a function of time, under the action of a single attosecond pulse of 40, 60, and 80 nm central wavelength and $N = 6$ cycles (the central time of the pulse is approximately 16.5, 25, and 33 a.u., respectively). The wells with potentials $W_\pm$ are located at ± 20 a.u., marked by horizontal dashed lines. The electronic ionization path predicted according to Eq. (6) (solid) and Eq. (7) (dashed) is indicated.

$$\frac{p^2(t)}{2} + V(\boldsymbol{r}(t)) = \omega + E_i. \quad (5)$$

Hence,

$$v(t) = p(t) = \{2[\omega + E_i - V(\boldsymbol{r}(t))]\}^{1/2}, \quad (6)$$

and ignoring the potential energy for electrons with large energy in the continuum, the velocity becomes time independent,

$$v(t) \approx v^{(0)} = [2(\omega + E_i)]^{1/2}. \quad (7)$$

Results for the action of one attosecond pulse with $\lambda = 40$ nm ($\hbar\omega = 1.14$), 60 nm (0.76), and 80 nm (0.57) are shown in Fig. 1 for $E_i = E_g$. The attosecond pulse has a duration of $N = 6$ cycles, and an intensity $I = 10^{16}$ W/cm^2. The classically calculated path of the electron is shown for both free electronic motion [dashed lines, Eq. (7)] and taking into account the nuclear potential [full lines, Eq. (6)]. While the free electron approximation is reasonably good for the most energetic electrons (40 nm) with excess energy of $\omega + E_g = 0.614$ (at a wavelength of 40 nm), it is not valid any more for the lower excess energy of 0.045 (80 nm).

The time evolution of the eigenstates under the influence of the total Hamiltonian given by Eq. (2) is

$$\psi_\pm^{\text{total}}(\boldsymbol{r},t) = U(t)\psi_\pm(\boldsymbol{r},0), \quad (8)$$

where $U(t)$ is the time-evolution operator. We can also define the time evolution of the eigenstates under H_0, which is time independent,

$$\psi_\pm(\boldsymbol{r},t) = U_0(t)\psi_\pm(\boldsymbol{r},0) \equiv \exp^{-(iH_0t)}\psi_\pm(\boldsymbol{r},0). \quad (9)$$

As a measure for the fraction of the electron wave packet, which gets recaptured at the left well W_-, we calculate the overlap of its eigenfunction $\psi_-(x,t)$ [see Eq. (4)] with the time-dependent wave packet

$$C_-(t) = \langle \psi_-(\boldsymbol{r},t) | \psi(\boldsymbol{r},t) \rangle, \quad (10)$$

which is formally a cross-correlation function.

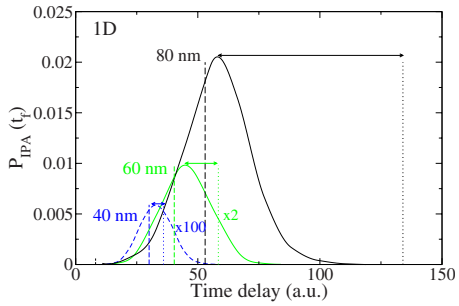

FIG. 2. (Color online) Probability of the induced photoassociation at W_- as a function of the delay between the pulses, for three photon wavelengths: $\lambda=40$, 60, and 80 nm (one-dimensional calculations). The predicted optimal delay according to Eqs. (6) and (7) is indicated with dashed and dotted lines, respectively. The arrows highlight the difference between the real and calculated values if the potential energy is ignored.

The probability for induced photoassociation (IPA) in the left well is therefore given by

$$P_{\mathrm{IPA}}(t) = |C_-(t)|^2. \tag{11}$$

The final population of W_- is $P_{\mathrm{IPA}}(t_f)$, where t_f is the time at the end of the second attosecond pulse, which is delayed by Δt with respect to the first one. As can be seen from Fig. 2, an optimum delay Δt^* for maximum IPA exists. Δt^* is reasonably predicted by the high photon energy approximation for 40 nm, but not for lower energies (dotted lines). However, the inclusion of the nuclear potential [Eq. (6), dashed lines] provides a good prediction for all three energies, with differences with respect to the real value of around 8% for 40 nm, and 10% for 60 and 80 nm. Note that larger wavelengths provide a worse accuracy in the predicted optimum delays, but correspond to higher absorption probabilities, which might be useful experimentally.

The experimental observation of IPA is possible by detecting the outgoing proton or electron flux. For optimal time delay sufficient absorption at W_- will lead to a decrease in the number of protons as well as the number of electrons detected in this direction (negative x axis).

To study the asymmetry in the electronic emission, we use the continuity equation

$$\frac{\partial|\Psi(\boldsymbol{r},t)|^2}{\partial t} = -\boldsymbol{\nabla}\boldsymbol{j}(\boldsymbol{r},t), \tag{12}$$

which relates the change in the electronic density as a function of time with the particle flux

$$\boldsymbol{j}(\boldsymbol{r},t) = \Re\left(\Psi^*(\boldsymbol{r},t)\frac{\hbar}{im}\boldsymbol{\nabla}\Psi(\boldsymbol{r},t)\right). \tag{13}$$

In one dimension, integration of Eq. (12) in space leads to

$$\int_{-L}^{L}\frac{\partial|\Psi(x,t)|^2}{\partial t}dx \equiv \frac{\partial N}{\partial t} = j(-L,t) - j(L,t), \tag{14}$$

where N is the number of electrons. Using Eq. (12) again for the right hand side of Eq. (14) yields

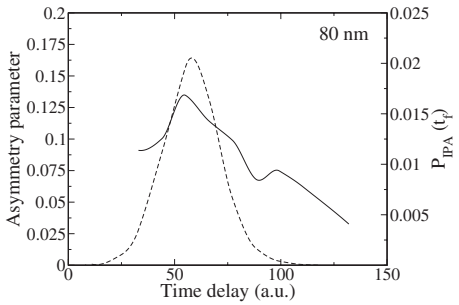

FIG. 3. Full line, asymmetry parameter as a function of the time delay [Eq. (16)], for $\lambda=80$ nm and the same laser parameters as in Fig. 2. Dashed line, IPA probability (population at W_-), shown for comparison.

$$\frac{\partial N}{\partial t} = \frac{\partial N_+}{\partial t} + \frac{\partial N_-}{\partial t}, \tag{15}$$

providing the ionization rate $\frac{\partial N}{\partial t}$ in terms of particles N_+ escaping to the right passing the position $+L$ and the ones N_- escaping to the left passing $-L$. We define the parameter

$$A = \frac{\Delta N_+ - \Delta N_-}{\Delta N_+ + \Delta N_-} \tag{16}$$

for asymmetric escape. If the electron is originally located in the well W_+ (at $+r_0$), the flux should ideally be symmetric if there is no absorption at W_-. With absorption at W_- located at $-r_0$, there should be less flux through $-L$ than through L, so that $A>0$. In Fig. 3 the asymmetry parameter for the two wells system is shown (full line) together with the IPA probability (dashed line, see also Fig. 2) for comparison. Indeed, A has a maximum if the population at the second well is maximal.

Note that the asymmetry parameter is never zero. The second well reflects part of the ionized wave function, resulting in a higher value of ionization flux toward the side where W_+ is located (positive x axis). For this reason the experimental detection of the reabsorption in W_- should be based on the shape of the asymmetry parameter, and not on its absolute value.

Our one-dimensional calculations suggest that electron population can be efficiently transferred to the second well W_- by optimizing the time delay between two attosecond pulses. The induced photoassociation probability as a function of the time delay can be used to measure the distance of the nuclei in the molecule. Furthermore, we have seen that the left and right asymmetry in the ionization signal could be a natural way to observe these effects in an experiment.

To substantiate these findings we have carried out more realistic 2D calculations, where spreading of the electronic wave packet in the coordinate transversal to the laser polarization is naturally included. Results shown in Fig. 4 are fully analogous to those of the one-dimensional case, although the IPA probabilities are obviously smaller, since the outgoing electron now has access to the transverse direction. The differences between obtained and predicted maxima ac-

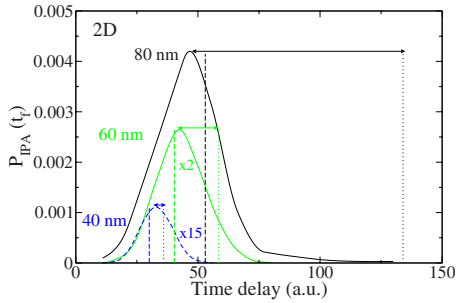

FIG. 4. (Color online) The same as Fig. 2 but in two dimensions.

cording to Eq. (6) are now 12% for 80 nm, 6% for 60 nm, and 9% for 40 nm.

IV. TWO ATTOSECOND PULSES PLUS INFRARED FIELD

So far we have demonstrated that the time delay between two attosecond pulses can be used to measure atomic distances, or to optimize the electronic transfer between two nuclei. However, with the current state-of-the-art technology, it is still difficult to isolate two pulses and choose the time delay between them.

Attosecond pulses are created [1] through high harmonic generation produced by the interaction of an IR laser field with an atom or molecule. With this technique one can easily generate attosecond pulse trains (APT), with one or two [12] attosecond pulses per infrared cycle of the generating field. For a Ti:Sa laser ($\lambda=800$ nm), the time delay between attosecond pulses is fixed to $T\sim 110$ or $T/2\sim 55$, and therefore the technique described in the previous section cannot be directly applied.

To overcome this limitation we will introduce, in addition to a fixed and realistic delay between attosecond pulses, a synchronized IR field. Due to the way the APT is generated, a synchronized IR pulse is always available.

The phase of the IR laser pulse can be chosen to either accelerate or decelerate the electron when it is released at the first well W_+ [14,15] and therefore it will influence the temporal and spatial overlap between the ionized electron and the second well W_- at the time of the second attosecond pulse.

In other words, an appropriate infrared field, applied while the electron travels the distance between the nuclei, can alter the electron trajectory such that the electron arrives at W_- when the second attosecond pulse is applied, thereby optimizing IPA.

Our electric field has from now on three contributions: two Gaussian attosecond pulses of intensity $I_{UV}=10^{15}$ W/cm^2 and FWHM$=2T$, and an infrared field

$$E_{IR}(t)=E_{IR}\sin(\omega_{IR}t+\phi)\sin^2\left(\frac{\omega_{IR}t}{2N_{IR}}\right) \tag{17}$$

with $N_{IR}=8$ and $I_{IR}=10^{13}$ W/cm^2. We have reduced the UV intensity by a factor of 10 compared to the previous section, to work out more clearly the IPA enhancement produced by the IR field. The two attosecond pulses, separated by an infrared period $\Delta t=T_{IR}$, are located symmetrically with respect to the center of the infrared. The central wavelength of the attosecond pulses is $\lambda=65$ nm ($\omega=0.7$). This implies that the optimal delay [following Eq. (7)] would be $t=2x_0/v\sim 68$, much less than the actual delay of $T=110$ between the pulses. Therefore, we expect enhanced recombination at W_- if the IR field decelerates the outgoing electron. To this end we vary the carrier-envelope phase of the infrared pulse ϕ in Eq. (17). This changes the value of the IR field at the moment when the electron is ionized by the first attosecond pulse and is equivalent to changing the time at which the attosecond pulses occur during the infrared pulse. The latter has already been achieved experimentally [16–18].

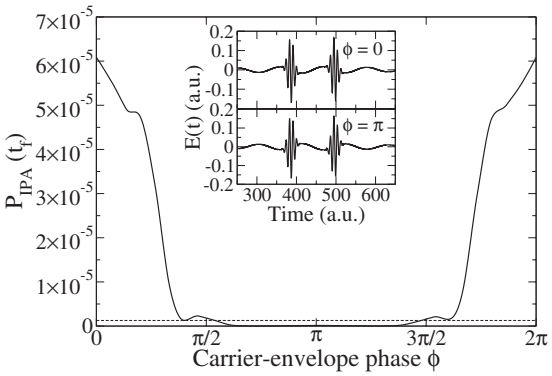

FIG. 5. Probability of the induced photoassociation at W_- as a function of the carrier-envelope phase of the infrared pulse. The insets show the total field for $\phi=0$ and π.

For the present intensity, the infrared pulse by itself causes negligible absorption at W_- of only $P_{IPA}\sim 10^{-13}$. This ensures that IPA comes from the attosecond pulse only, while the infrared pulse has exclusively the role of accelerating or decelerating the ionized electrons. Results for IPA in the second well as a function of the carrier-envelope phase of the infrared pulse are shown in Fig. 5. The insets show the position of the attosecond pulses with respect to the infrared pulse, for the cases with $\phi=0$ and $\phi=\pi$. The dashed line close to the bottom of the figure ($P_{IPA}\sim 1.275\times 10^{-6}$) corresponds to the case in which only the attosecond pulses, but not the infrared, are acting on the system. It illustrates impressively the enormous capability of the infrared pulse to steer the ionized electron, thereby dramatically changing IPA: for $\phi=0$ the photoassociation probability is ~ 50 higher than without the infrared, while for $\phi=0.73\pi$ it is around 37 times smaller. The contrast between maximum ($\phi=0$) and minimum ($\phi=\pi$) is therefore ~ 1850 rendering this mechanism very efficient. Figure 6 illustrates the effect of the IR field on attosecond-induced photoassociation. It shows the change in the electron trajectory due to the infrared field, for $\phi=0$ and π, together with the expected trajectory of the electron under the influence of the two nuclei and the IR field. These trajectories have been calculated with Eq. (6), where now $V_{IR}(x(t))=V+xE_{IR}(t)$, i.e., the interaction is given by the original potential V from Eq. (2) with the IR field added.

With $\phi=0$, the electron is maximally decelerated. It arrives later at the second well, enhancing the recombination

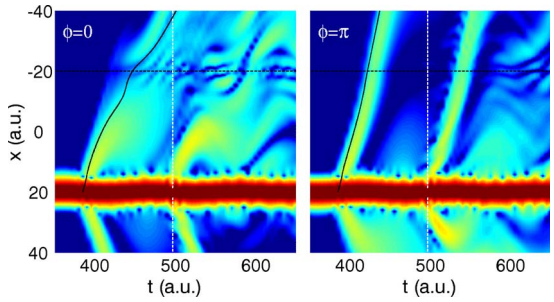

FIG. 6. (Color online) Bending of the electron trajectory caused by the infrared field ($\lambda=800$ nm, $I=10^{13}$ W/cm^2). Left, with carrier-envelope phase $\phi=0$ in the infrared pulse (see the insets in Fig. 5). Right, the same situation when $\phi=\pi$. Dashed black line, position of the nucleus W_-. Dashed white line, position of the center of the second attosecond pulse. Full line, expected trajectory following Eq. (6).

probability. For $\phi=\pi$ the effect is a slight acceleration: the electron arrives even earlier at the second well, hence the IPA probability is vanishingly small. This can be seen even more clearly in Fig. 7 in terms of classical trajectories of the electron for the cases shown in Fig. 6. From there it is clear that the optimum situation for IPA (coincidence in space and time of electron trajectory, second well position and peak of second attosecond pulse) cannot be reached for the present parameters chosen, which was done on purpose to provide a "typical" situation.

V. TRAIN OF ATTOSECOND PULSES

The combination of two attosecond pulses and an IR pulse as discussed in the previous section can enhance the IPA probability. Yet, it is still small, especially considering that in one dimension the recombination probabilities are unrealistically increased due to the absence of wave packet spreading in the transversal direction. One may overcome this problem by using more than two attosecond pulses. With more pulses in the train and a longer IR pulse, the transfer process is repeated each cycle, thus increasing the net probability of recombination at W_-. From the experimental point of view, longer APT are even easier to generate and to handle.

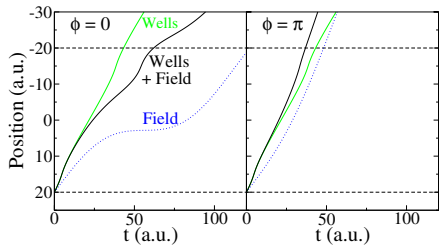

FIG. 7. (Color online) Electron trajectories calculated with Eq. (6) in the presence of the wells (dashed lines), the infrared field (dotted lines), or both of them (full lines), for carrier-envelope phases of $\phi=0$ or $\phi=\pi$. The position of the wells is indicated by the dashed lines. The origin in time is the center of the first attosecond pulse.

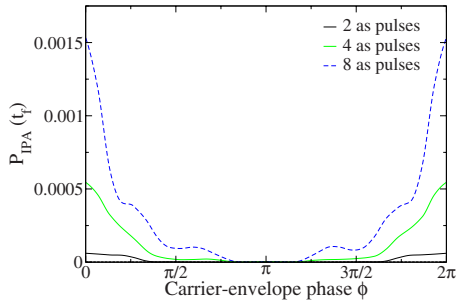

FIG. 8. (Color online) Probability of induced photoassociation at W_- as a function of the carrier-envelope phase of the infrared pulse, for 2, 4, and 8 attosecond pulses in the train. Intensities, $I_{IR}=10^{13}$ W/cm^2, and $I_{UV}=10^{15}$ W/cm^2.

After the second pulse in the train, the population at the second well is nonzero. Hence, for any further pulse, there will be ionization from both wells. Yet, given a fixed ionization probability p, there is a net increase of population at W_-, because initially the probability at W_+ is much larger than at W_-.

For n pulses, a simple estimate of the population probabilities at W_+ and W_- yields

$$A_n^+ = A_{n-1}^+(1-p) + A_{n-2}^- p^2,$$

$$A_n^- = A_{n-1}^-(1-p) + A_{n-2}^+ p^2. \tag{18}$$

If initially the first well is occupied ($A_0^+=1$) and the second well is empty ($A_0^-=0$), the population of the second well as a function of the number of pulses n will evolve to a maximum whose position depends on the value of p. In our case, the first attosecond pulse induces an ionization of about 3.64% of the initial state, thus $p=0.0364$ and the maximum appears at $n=29$. In Fig. 8 we show the IPA in W_- versus the carrier-envelope phase for numerical calculation using an APT containing 2, 4, or 8 pulses. By increasing the number of attosecond pulses, the absorption can be better controlled: for two pulses the enhancement factor at $\phi=0$ with respect to the case without IR is 50 (as seen in Fig. 5) increasing to 480 and 1530 for 4 and 8 pulses, respectively.

VI. CONCLUSIONS AND OUTLOOK

We have introduced the process of attosecond pulse-induced photoassociation. For that purpose, a pump-probe scheme of attosecond pulses has been used in a system consisting of a dissociating H_2^+ molecule with the electron initially located in one of the ions. The pump pulse ionizes the electron and the probe pulse can induce the reabsorption at the other ion when the delay between the pulses corresponds to the time the electron needs to reach the second ion.

We have proven that the IPA probability can be controlled by changing the delay between the pulses. We have also discussed and analyzed two experimental feasible ways for enhancing this probability: the use of an infrared pulse to accelerate or decelerate the electron, and the use of a train of attosecond pulses instead of a single pair, to maximize the

charge transfer between them. Both ways are shown to enhance IPA considerably. Furthermore, the experimental detection of reabsorption is facilitated through a study of the forward or backward asymmetry of the electronic flux along the polarization direction.

Deliberately, we have chosen the laser parameters and the distances of, as well as the binding energies at the atomic centers such that the resulting dynamics can be described quasiclassically, providing an intuitive picture in terms of classical trajectories guiding the electronic wave packets. This has been important to allow for a straightforward interpretation of the IPA results, as presented here. In fact, IPA dynamics is far more intricate, especially outside the quasiclassical regime, e.g., if the excess energy of the electronic wave packet is small (due to a small frequency of the attosecond pulses or a large binding energy, as studied for an atom in [16]). Future work on more than one atomic center will engage in this direction with the chance to uncover so far unknown effects.

Moreover, our ideas can be extended to more complex molecules, where several centers may exist, opening new possibilities to carry out microscopic time-of-flight measurements to explore microscopic spatial landscapes. This will be especially useful in situations where the static and well developed diffraction methods fail due to a fast change of the microscopic landscape, e.g., a fast explosion or reorganization of the ions in a large molecule.

ACKNOWLEDGMENTS

We acknowledge contributions by S. Baier, A. Becker, F. He, P. Panek, and A. Requate to the virtual laser laboratory Nonlinear Processes in Strong Fields Library, which has been used for the present calculations. P.R. acknowledges the Ministerio de Educación y Ciencia (Spain).

[1] P. M. Paul *et al.*, Science **292**, 1689 (2001).
[2] R. López-Martens *et al.*, Phys. Rev. Lett. **94**, 033001 (2005).
[3] P. Corkum *et al.*, Nat. Phys. **3**, 381 (2007).
[4] R. Kienberger *et al.*, Science **297**, 1144 (2002).
[5] Y. Nabekawa, T. Shimizu, T. Okino, K. Furusawa, H. Hasegawa, K. Yamanouchi, and K. Midorikawa, Phys. Rev. Lett. **96**, 083901 (2006).
[6] M. F. Kling *et al.*, Science **312**, 246 (2006).
[7] F. He, C. Ruiz, and A. Becker, Phys. Rev. Lett. **99**, 083002 (2007).
[8] M. Uiberacker *et al.*, Nature (London) **446**, 627 (2007).
[9] T. Remetter *et al.*, Nat. Phys. **2**, 323 (2006).
[10] M. Drescher *et al.*, Nature (London) **419**, 803 (2002).
[11] J. Itatani *et al.*, Nature (London) **432**, 867 (2004).
[12] J. Mauritsson, P. Johnsson, E. Gustafsson, A. L'Huillier, K. J. Schafer, and M. B. Gaarde, Phys. Rev. Lett. **97**, 013001 (2006).
[13] S. X. Hu and L. A. Collins, Phys. Rev. Lett. **96**, 073004 (2006).
[14] P. Johnsson *et al.*, Phys. Rev. Lett. **95**, 013001 (2005).
[15] F. Remacle, M. Nest, and R. D. Levine, Phys. Rev. Lett. **99**, 183902 (2007).
[16] P. Johnsson, J. Mauritsson, T. Remetter, A. L'Huillier, and K. J. Schafer, Phys. Rev. Lett. **99**, 233001 (2007).
[17] I. D. Williams *et al.*, Phys. Rev. Lett. **99**, 173002 (2007).
[18] L. Miaja-Avila, C. Lei, M. Aeschlimann, J. L. Gland, M. M. Murnane, H. C. Kapteyn, and G. Saathoff, Phys. Rev. Lett. **97**, 113604 (2006).
[19] Note that in three dimensions, $\psi_{g/u}$ are given by the ground state $1s\sigma_g$ and first excited state $2p\sigma_u$ molecular orbitals.